# Polygonal tessellations as predictive models of molecular monolayers

Krisztina Regős[a,b,1], Rémy Pawlak[c] [ID], Xing Wang[d], Ernst Meyer[c], Silvio Decurtins[d] [ID], Gábor Domokos[a,b], Kostya S. Novoselov[e,1] [ID], Shi-Xia Liu[d,1] [ID], and Ulrich Aschauer[c,1,2]

Molecular self-assembly plays a very important role in various aspects of technology as well as in biological systems. Governed by covalent, hydrogen or van der Waals interactions–self-assembly of alike molecules results in a large variety of complex patterns even in two dimensions (2D). Prediction of pattern formation for 2D molecular networks is extremely important, though very challenging, and so far, relied on computationally involved approaches such as density functional theory, classical molecular dynamics, Monte Carlo, or machine learning. Such methods, however, do not guarantee that all possible patterns will be considered and often rely on intuition. Here, we introduce a much simpler, though rigorous, hierarchical geometric model founded on the mean-field theory of 2D polygonal tessellations to predict extended network patterns based on molecular-level information. Based on graph theory, this approach yields pattern classification and pattern prediction within well-defined ranges. When applied to existing experimental data, our model provides a different view of self-assembled molecular patterns, leading to interesting predictions on admissible patterns and potential additional phases. While developed for hydrogen-bonded systems, an extension to covalently bonded graphene-derived materials or 3D structures such as fullerenes is possible, significantly opening the range of potential future applications.

tessellation | self-assembly | monolayer | 2D

Two-dimensional (2D) natural patterns at all scales, ranging from molecular assemblies (1, 2) to macroscopic entities (3, 4), often appear as polygonal tessellations (5). The corresponding mathematical theory (6, 7) could be harnessed to obtain a deeper understanding of the structure-forming process. Our aim here is to make this step for molecular monolayers. Supramolecular tessellation in these materials is often based on noncovalent van der Waals interactions or halogen- and hydrogen bonding between neighboring molecules (8–11, 12). Illustrative examples of the former interactions are tessellations via exo-wall contacts between shape-persistent polygonal macrocycles, such as pillar[6]arene, which have a hexagonal configuration leading to a trivalent vertex (13). Similarly, 2D layered network superstructures have been formed using pagoda[4]arene with square and rhombic tiles (14). Supramolecular tessellation studies based on directional hydrogen bonding are numerous, as the extended structures can be varied over a wide range by careful design of the molecular building blocks (15–17). Although in recent decades empirical insights into the molecular self-assembly patterns are increasingly obtained from experimental scanning tunneling microscopy data at molecular resolution that often allow for an intuitive assessment of the resulting molecular tiles, theoretical methods leading to a deeper understanding and predictability of pattern formation are still urgently needed.

Theoretical investigations have shown the architecture and symmetry of the molecular precursor to play an important role in combination with the nature of the intermolecular interactions (18). In a recent study, Baran et al. investigated how the two important factors of complementary molecular size and shape in combination with the presence of directed interactions control self-assembly at the surface (19, 20). Using coarse-grained modeling, their study aims to both reproduce experimental data and predict new supramolecular structures, thereby gaining an understanding of the factors playing a key role in the self-assembly process. In addition, molecular dynamics, and related computational approaches, have been applied to various molecular architectures (21, 22). Despite continuous advances in efficient algorithms and computational speed, reorientation kinetics are often too slow to capture all possible configurations and reliably identify the most stable structure. Enhanced sampling and Monte Carlo (22, 23) or machine learning (18, 24) approaches have alleviated this issue but still require significant computational resources.

## Significance

Pattern prediction of two dimensions (2D) molecular networks has so far relied on computationally involved approaches such as density functional theory, classical molecular dynamics, Monte Carlo, or machine learning. Here, we demonstrate an apparently simpler approach: Based on the mean-field theory of 2D polygonal tessellations, we build a hierarchical geometric model for supramolecular pattern classification and prediction. When applied to existing experimental data, our model provides a different view of self-assembled molecular patterns, leading to interesting predictions about admissible patterns and potential additional phases. While developed for hydrogen-bonded systems, an extension to covalently bonded graphene-derived materials or 3D structures such as fullerenes is possible, significantly opening the range of potential future applications.

[1]To whom correspondence may be addressed. Email: regos.kriszti@gmail.com, kostya@manchester.ac.uk, shi-xia.liu@unibe.ch, or ulrich.aschauer@unibe.ch.

[2]Present address: Department of Chemistry and Physics of Materials, University of Salzburg, A-5020 Salzburg, Austria.

## Results and Discussion

In this work, we present an alternative theoretical approach based on the mean-field theory of space-filling polygonal mosaics (6, 25, 26), which describes these structures by average values $\bar{n}$, $\bar{v}$ of the nodal and cell degrees. The former counts the number of polygons meeting at one vertex, and the latter counts the number of vertices of a polygon (Fig. 1). The averages $\bar{n}$, $\bar{v}$ span the symbolic plane and each space-filling mosaic is associated with one point on this plane. This representation proved useful in determining the provenance of natural fragmentation patterns (3, 4). As compared to fracture patterns, molecular assemblies show special features: If they are space filling, they are also regular (i.e., the vertex of one polygon is not admitted lying in the interior of an edge of another polygon) in which case the averages are not independent (25, 26):

$$\bar{v} = \frac{2\bar{n}}{\bar{n} - 2}, \tag{1}$$

therefore, if one of the averages can be predicted, the other may be computed using Eq. **1**.

Single-layer materials may be represented by a hierarchical geometric model, consisting of (parts of) polygonal mosaics on multiple scales, which we dub levels and denote, in hierarchical order, by $L_i$, ($i = 1,2,3,4$), associated with the averages $\bar{n}_i$, $\bar{v}_i$. We note that the concept of levels was first introduced to describe the fractal geometry of 2D foams (27). Our approach is conceptually similar in the sense that scales of subsequent levels are well separated; however, in our case, the subsequent levels do not carry self-similar patterns. Instead of being interpreted as convex mosaics, levels may also be viewed as graph representations of the monolayer. In this context, levels $L_2$ and $L_4$ emerge as the two essential models, being, respectively, the fully expanded and the fully contracted graphs associated with the monolayer. We next illustrate these levels on the example of the α-phase of the 2,7-pyrenedione (PO) molecule (*SI Appendix*, section S1.1) as shown in Fig. 2.

Level $L_1$ is not space filling and describes the geometry of the interacting sites of a single molecule as a convex polygon with $\bar{v}_1$ vertices at the molecule's perimeter atoms (i.e., the atoms able to form intermolecular bonds). For the PO example, we have $\bar{v}_1 = 10$ (eight hydrogen and two oxygen atoms). In addition, we also characterize the chemical bonding of the molecule via the parameters $b_1$ and $\hat{b}_1$. For the hydrogen-bonded systems we focus on, $b_1$ is the maximum acceptor capacity of any atom among the $\bar{v}_1$ perimeter atoms. For PO, $b_1 = 2$, i.e., the maximum number of accepted hydrogen bonds for the oxygen atom. Based on the molecule's total number of accepted ($b_a$) and donated ($b_d$) hydrogen bonds, we define $\hat{b}_1 = \min(b_a,\ b_d)$. For
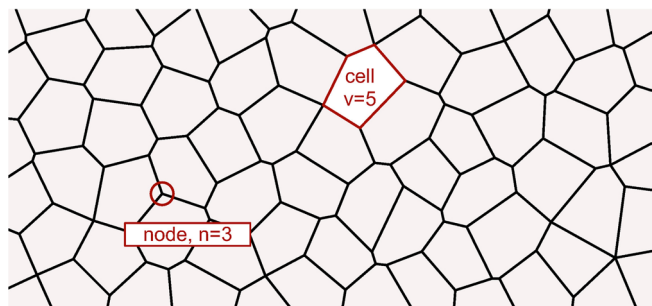
PO, $b_a = 4$ (two oxygen atoms with two accepted bonds each) and $b_d = 8$ (eight hydrogen atoms with one donated bond each), so $\hat{b}_1 = \min(4, 8) = 4$ (Fig. 3).

Levels $L_2$, $L_3$, and $L_4$ describe supramolecular space-filling tessellations, so formula (**1**) can be used and in each case the single average $\bar{n}_i$ characterizes the pattern. As noted, level $L_2$ is an essential model characterized by the fully expanded graph: Here, all perimeter atoms appear as nodes and besides the edges of the $L_1$–polygons (molecular perimeter), all intermolecular bonds appear as edges (Fig. 2). On level $L_2$, we also define as $b_2$ the average number of bonds between neighboring molecules. For the PO α-phase, the nodal and cell degree averages are $(\bar{n}_2,\ \bar{v}_2) = (2.633, 8.316)$, and the average bonding number $b_2 = 1.357$. We derive the graph corresponding to level $L_3$ from level $L_2$ via chemically targeted face contractions: All faces of the $L_2$ graph (i.e., cells of the $L_2$ mosaic) corresponding to molecules are contracted to single nodes (Fig. 2), such that, on level $L_3$, the nodes are the molecules, and each intermolecular bond is counted as an edge. For the PO α-phase, we have nodal and cell degree averages $(\bar{n}_3,\ \bar{v}_3) = (6.333, 2.923)$, and level $L_4$, finally, is again an essential model, characterized by the fully contracted graph. The latter is, as before, obtained from the preceding level $L_3$ via chemically targeted face contractions: All faces of the $L_3$ graph (cells of the $L_3$ mosaic), the perimeter of which is formed by two intermolecular bonds, are contracted to single edges (Fig. 2), so, on level $L_4$, the nodes are the molecules, and a single edge is added for any two bonded molecules, independent of the number of bonds they share. For the PO α-phase, $(\bar{n}_4,\ \bar{v}_4) = (4.667, 3.500)$.

These definitions can be used to organize supramolecular patterns using the symbolic plane. Fig. 4 shows the level $L_2$ patterns associated with some 2D materials (to be discussed in more detail below and in *SI Appendix*, section S1) as well as some simple periodic patterns in the symbolic plane along the curve defined by Eq. **1**.

The model can be made predictive by expressing the supramolecular pattern averages $\bar{n}_2, \bar{n}_3, \bar{n}_4$ by the molecular pattern average $\bar{v}_1$ and the chemical bonding information carried by the constants $b_1$, $\hat{b}_1$, and $b_2$. While the derivation can be found in *SI Appendix*, section S2, we here present the formulae along with some physical interpretation. Formulae (**2**), (**3**), and (**4**) determine higher-level geometric information based on lower-level geometric and chemical information:

$$\frac{2}{\bar{v}_1} + 2 \leq \bar{n}_2 \leq \frac{2\hat{b}_1}{\bar{v}_1} + 2 \leq \frac{2b_1}{b_1 + 1} + 2, \tag{2}$$

$$\bar{n}_3 = \bar{v}_1(\bar{n}_2 - 2), \tag{3}$$

$$\bar{n}_4 = \frac{\bar{n}_3}{b_2}. \tag{4}$$

In addition, the mixed formula (**5**), expresses mean-field averages using both lower-level and higher-level information:

$$\frac{\bar{n}_4}{\bar{v}_1} + 2 \ \leq \ \bar{n}_2. \tag{5}$$

We note that if the level 4 pattern is convex, then in formula (**5**), $\bar{n}_4 \geq 3$. The geometric model formed by formulae (**2–5**) was found to be correct for the experimental data of 2D ice as well as 2,7-dihydroxypyrene (PO), 1,6,7,12-tetraazaperylene (TAPE) and triimidazo[1,3,5]triazine (TT) molecules (see data points in Fig. 4
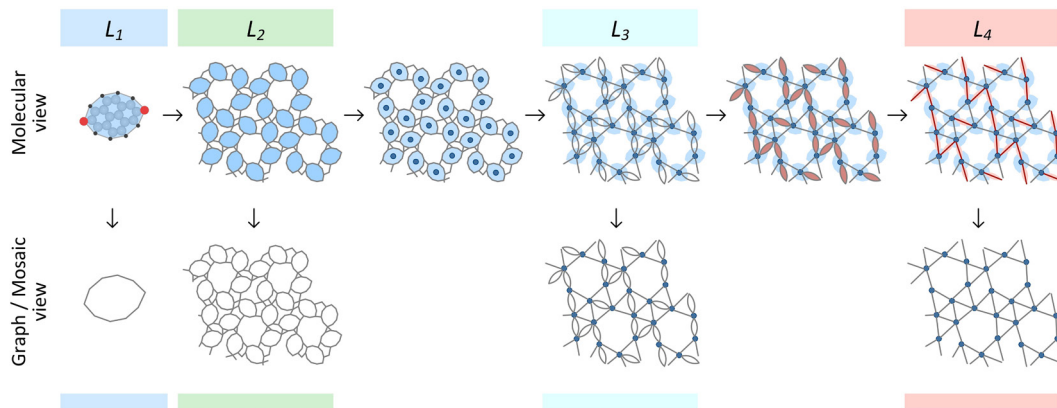


**Fig. 1.** Regular polygonal mosaic in the plane. The cell degree *v* counts the vertices of a polygon, the nodal degree *n* counts the polygons overlapping at a vertex.

**Fig. 2.** Illustration of the levels as an interpretation of molecular patterns, using the α-phase of the 2,7-pyrenedione (PO) molecule. *Upper* row: Physical images of molecules and patterns. *Lower* row: Abstract graph/mosaic representation of patterns. Columns: Level $L_1$: Structure of the molecule and blue polygon derived from the perimeter atoms (*Upper* row), perimeter as convex polygon (*Lower* row). Level $L_2$: Supramolecular pattern. Faces corresponding to molecules are filled with blue color (*Upper* row) and shown in graph representation (*Lower* row). Level $L_2 \rightarrow L_3$ transition shown in the *Upper* row: Midpoint of blue molecular faces marked as new nodes. Level $L_3$: Pattern obtained by contracting blue molecular faces to single nodes. *Lower* row: Graph of level $L_3$. Level $L_3 \rightarrow L_4$ transition shown in the *Upper* row: Faces between multiple adjacent bonds are colored red. Level $L_4$: Pattern obtained by contracting red faces to edges. *Lower* row: Graph of level $L_4$.

and *SI Appendix*, section S1 for numeric values as well as a description of the molecules). We note that formula (**2**), and particularly the right-most upper bound, predicts that $\overline{n}_2 \leq 4$ and consequently $\overline{v}_2 \geq 4$ for all level $L_2$ supramolecular patterns. This implies for all conceivable supramolecular patterns $\overline{n}_2 \leq \overline{v}_2$, thus lying toward the left on the curve given by formula (**1**), greatly restricting the variety of possible patterns. In addition, we found that the bounds given by Eqs. **2** and **5** are sharp, i.e., there exist known 2D molecular monolayers where these bounds are exactly realized. This can be seen for the case of 2D ice in Fig. 4, where the hexagonal and square arrangements lie on the upper and lower bounds, respectively, of the admissible range (shown by the red arrow) determined by a combination of formula (**5**) for the lower and formula (**2**) for the upper bound:

$$\frac{3}{\overline{v}_1} + 2 \leq \overline{n}_2 \leq \frac{2\widehat{b}_1}{\overline{v}_1} + 2.$$ [6]

In formula (**5**), we used the information that the level $L_4$ pattern is convex. This implies that these bounds cannot be improved unless one imposes restrictions on the set of considered materials.

One notable feature of the admissible ranges for water and PO shown in Fig. 4 is that they do not overlap on either axis, implying
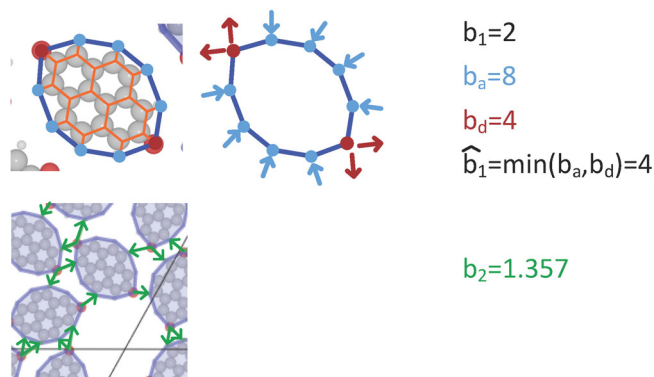


**Fig. 3.** Chemical information used in formulae (**2–4**), for the example of the α-phase of the 2,7-pyrenedione (PO) molecule. Upper image: Maximum acceptor capacity $b_1$ of any atom among the perimeter atoms as well as the molecule's total number of accepted ($b_a$) and donated ($b_d$) hydrogen bonds and $\widehat{b}_1 = \min(b_a, b_d)$. Lower figure: $b_2$ as the average number of bonds between neighboring molecules.

that the two molecules will never produce identical supramolecular patterns.

Apart from the PO α-phase, mentioned in deriving the levels, the same molecule may also form a β-phase, which is characterized by a slightly larger $\overline{n}_2$. Neither of the two phases, however, lies on the boundary of the admissible range (shown by the purple arrow), implying that further phases could exist. While no structure outside the range delimited by the α- and β-phases was observed experimentally, a γ-phase falling within this range was observed, which has $(\overline{n}_4, \overline{v}_4) = (3.600, 4.500)$. We observe a potentially interesting symmetry at level $L_4$: the α- and β-phases correspond to the symmetrical, dual points $(\overline{n}_4, \overline{v}_4)$ at $(4.667, 3.500)$ and $(3.500, 4.667)$, respectively (*SI Appendix*, section S1). The underlying physical meaning of this symmetry uncovered by our mean-field geometric model and its validity for other molecular architectures will be an interesting topic for future research.

A further interesting aspect is that the model may be tuned by adding additional data to the chemical bonding information. Temperature influences the bonding constant $\widehat{b}_1$ and, via Eq. **2**, also the combinatorial averages. For PO, $\widehat{b}_1$ has been computed via Boltzmann populations based on density functional theory (DFT) total energies of single and bifurcate hydrogen bonds (see details in *SI Appendix*, section S3). As the preference for bifurcate hydrogen bonds is reduced with increasing temperature, $\widehat{b}_1$ decreases and the lower bound for $\overline{v}_2$ increases as a function of temperature (*SI Appendix*, Fig. S4). This implies that at finite temperature the admissible range for patterns may shrink.

## Conclusion

In summary, we have applied the theory of space-filling polygonal tessellations to classify 2D molecular monolayers and obtained a predictive understanding of the conceivable geometries. While developed here for hydrogen-bonded molecular networks, there is no fundamental reason restricting our method to this class of materials. Indeed, only the higher upper bound in Eq. **2** is directly related to hydrogen bonding, while the rest of the model could be readily applied to other 2D assemblies; for example, covalently bonded atomic systems like the rich class of graphene-derived compounds such as porous and doped graphene (29) or related compounds such as boron nitrate (30) or borophene (31). As the concept of the $(\overline{n}, \overline{v})$ symbolic plane does not depend on the dimension of the tessellation, the same concepts could, in principle,
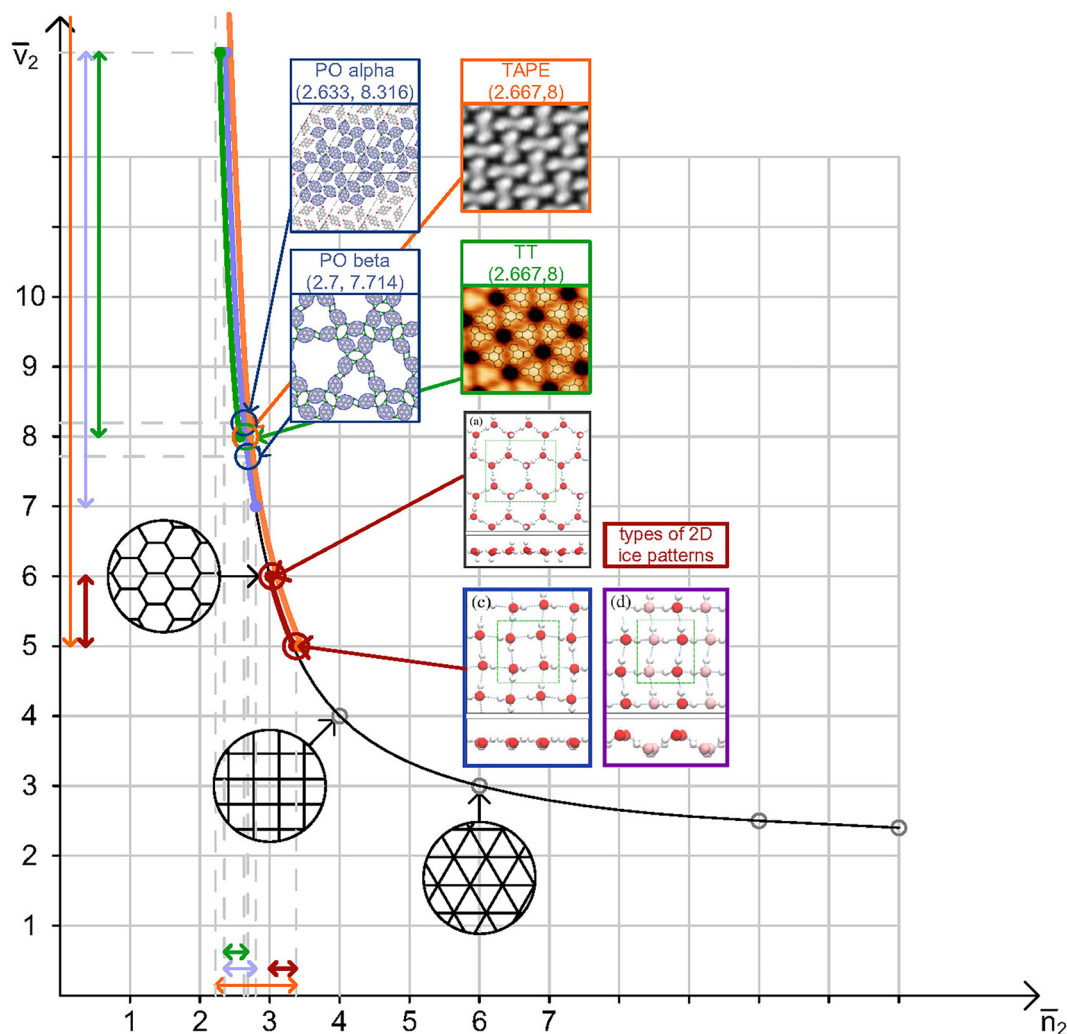
**Fig. 4.** Level $L_2$ supramolecular patterns organized along the line of Eq. **1** in the symbolic plane. 2D ice structures adapted from ref. 28.

be applied to the classification of 3D supramolecular patterns. However, in 3D, no formula analogous to (**1**) exists, so we expect that patterns would occupy not just a curve, but a domain of the symbolic plane. Our theory has shown its promise for the classification and separation of 2D molecular networks. Given that our approach yields a set of numbers classifying any given molecule and assembly, it could be of high relevance in machine-learning studies of the temperature-dependent relation between molecular structure and the resulting assembly, serving as a preprocessing step to turn image data into suitable numerical datasets.

**Data, Materials, and Software Availability.** Density functional theory data and analysis is available at DOI: 10.24435/materialscloud:e4-h1 (32). All study data are included in the article and/or *SI Appendix*.

Author affiliations: [a]Department of Morphology and Geometric Modeling, Budapest University of Technology and Economics H-1111 Budapest, Hungary; [b]Morphodynamics Research Group, Eötvös Lóránd Research Network and Budapest University of Technology and Economics, H-1111 Budapest, Hungary; [c]Department of Physics, University of Basel 4056 Basel, Switzerland; [d]Department of Chemistry, Biochemistry and Pharmacy, University of Bern 3012 Bern, Switzerland; and [e]Institute for Functional Intelligent Materials, National University of Singapore, Singapore 117544, Singapore

Author contributions: K.R., S.D., G.D., K.S.N., S.-X.L., and U.A. designed research; K.R. and G.D. developed the geometric model; K.R., R.P., X.W., G.D., and U.A. performed research; K.R., R.P., X.W., E.M., S.D., G.D., K.S.N., S.-X.L. and U.A. analyzed data; and K.R., S.D., G.D., K.S.N., S.-X.L., and U.A. wrote the paper.

1. D. Écija *et al.*, Five-vertex archimedean surface tessellation by lanthanide-directed molecular self-assembly. *Proc. Natl. Acad. Sci. U.S.A.* **110**, 6678–6681 (2013).
2. Y. Beldjoudi *et al.*, Supramolecular tessellations by a rigid naphthalene diimide triangle. *J. Am. Chem. Soc.* **141**, 17783–17795 (2019).
3. P. Fratzl, O. Kolednik, F. D. Fischer, M. N. Dean, The mechanics of tessellations–bioinspired strategies for fracture resistance. *Chem. Soc. Rev.* **45**, 252–267 (2016).
4. G. Domokos, D. J. Jerolmack, F. Kun, J. Török, Plato's cube and the natural geometry of fragmentation. *Proc. Natl. Acad. Sci. U.S.A.* **117**, 18178–18185 (2020).

5.  P. Ball, *The Self-Made Tapestry: Pattern Formation in Nature* (Oxford University Press, 2001).
6.  B. Grünbaum, G. C. Shephard, *Tilings and Patterns: An Introduction* (W.H. Freeman, 1989).
7.  G. Domokos, Á. G. Horváth, K. Regős, A two-vertex theorem for normal tilings. *Aequationes Math.* **97**, 185–197 (2023).
8.  Q. Fan, J. M. Gottfried, J. Zhu, Surface-catalyzed C-C covalent coupling strategies toward the synthesis of low-dimensional carbon-based nanostructures. *Acc. Chem. Res.* **48**, 2484–2494 (2015).
9.  X. Bouju, C. Mattioli, G. Franc, A. Pujol, A. Gourdon, Bicomponent supramolecular architectures at the vacuum-solid interface. *Chem. Rev.* **117**, 1407–1444 (2017).
10. Y.-Q. Zhang *et al.*, Complex supramolecular interfacial tessellation through convergent multi-step reaction of a dissymmetric simple organic precursor. *Nat. Chem.* **10**, 296–304 (2018).
11. F. Cheng *et al.*, Two-dimensional tessellation by molecular tiles constructed from halogen–halogen and halogen–metal networks. *Nat. Commun.* **9**, 4871 (2018).
12. L. Feng *et al.*, Supramolecular tessellations at surfaces by vertex design. *ACS Nano* **13**, 10603–10611 (2019).
13. M. Li *et al.*, Supramolecular tessellations via pillar[n]arenes-based exo-wall interactions. *J. Am. Chem. Soc.* **142**, 20892–20901 (2020).
14. X.-N. Han, Y. Han, C.-F. Chen, Supramolecular tessellations by the exo-wall interactions of pagoda[4] arene. *Nat. Commun.* **12**, 6378 (2021).
15. A. Ciesielski *et al.*, Concentration-dependent supramolecular engineering of hydrogen-bonded nanostructures at surfaces: Predicting self-assembly in 2D. *J. Am. Chem. Soc.* **135**, 6942–6950 (2013).
16. A. G. Slater, L. M. A. Perdigão, P. H. Beton, N. R. Champness, Surface-based supramolecular chemistry using hydrogen bonds. *Acc. Chem. Res.* **47**, 3417–3427 (2014).
17. Z. Tao *et al.*, Construction of molecular regular tessellations on a Cu(111) surface. *Chem. Commun.* **54**, 7010–7013 (2018).
18. A. Jeindl *et al.*, Nonintuitive surface self-assembly of functionalized molecules on Ag(111). *ACS Nano* **15**, 6723–6734 (2021).
19. Ł Baran, D. Nieckarz, P. Szabelski, W. Rżysko, Controlling of the 2D self-assembly process by the variation of molecular geometry. *J. Phys. Chem. C* **123**, 19549–19556 (2019).
20. Ł Baran, W. Rżysko, Application of a coarse-grained model for the design of complex supramolecular networks. *Mol. Syst. Des. Eng.* **5**, 484–492 (2020).
21. V. Barone, M. Casarin, D. Forrer, S. Monti, G. Prampolini, Molecular dynamics simulations of the self-assembly of tetraphenylporphyrin-based monolayers and bilayers at a silver interface. *J. Phys. Chem. C* **115**, 18434–18444 (2011).
22. G. Copie *et al.*, Atomic scale modeling of two-dimensional molecular self-assembly on a passivated Si surface. *J. Phys. Chem. C* **118**, 12817–12825 (2014).
23. J. van der Lit *et al.*, Modeling the self-assembly of organic molecules in 2D molecular layers with different structures. *J. Phys. Chem. C* **120**, 318–323 (2016).
24. M. Ziatdinov, A. Maksov, S. V. Kalinin, Learning surface molecular structures via machine vision. *npj Comput. Mater.* **3**, 31 (2017).
25. R. Schneider, W. Weil, *Stochastic and Integral Geometry* (Springer, Berlin/Heidelberg, 2008).
26. G. Domokos, Z. Lángi, On some average properties of convex Mosaics. *Exp. Math.* **31**, 783-793 (2022). 10.1080/10586458.2019.1691090
27. T. Herdtle, H. Aref, Relaxation of fractal foam. *Phil. Mag. Lett.* **64**, 335–340 (1991).
28. J. Chen, G. Schusteritsch, C. J. Pickard, C. G. Salzmann, A. Michaelides, Two dimensional ice from first principles: Structures and phase transitions. *Phys. Rev. Lett.* **116**, 025501 (2016).
29. R. Pawlak *et al.*, On-surface synthesis of nitrogen-doped Kagome graphene. *Angew. Chem. Int. Ed. Engl.* **60**, 8370–8375 (2021).
30. L. H. Li, Y. Chen, Atomically thin boron nitride: Unique properties and applications. *Adv. Funct. Mater.* **26**, 2594–2608 (2016).
31. A. J. Mannix *et al.*, Synthesis of borophenes: Anisotropic, two-dimensional boron polymorphs. *Science* **350**, 1513–1516 (2015).
32. K. Regős *et al.*, Polygonal tessellations as predictive models of molecular monolayers. *Materials Cloud Archive*. https://archive.materialscloud.org/record/2023.48. Deposited 22 March 2023.